Composites Part C: Open Access 17 (2025) 100580

Contents lists available at ScienceDirect

Composites Part C: Open Access

journal homepage: www.sciencedirect.com/journal/composites-part-c-open-access

Large-area high thermal conductivity graphite-carboxymethylcellulose film easily produced by mechanical exfoliation of natural graphite using a three-roll mill

Junhao Wang [a], Hongsheng Lin [a], Jonathon D. Tanks [b], Yoshihiko Arao [c,d,*]

[a] Graduate School of Waseda University, Department of Applied Mechanics and Aerospace Engineering, 3-4-1 Okubo, Shinjuku, Tokyo, Japan
[b] National Institute for Materials Science, Research Center for Structural Materials, 1-2-1 Sengen, Tsukuba, Ibaraki, Japan
[c] Waseda University, Department of Applied Mechanics and Aerospace Engineering, 3-4-1, Okubo, Shinjuku, Tokyo, Japan
[d] Kagami Memorial Research Institute for Materials Science and Technology, Waseda University, 2-8-26 Nishiwaseda, Shinjuku-ku, Tokyo, Japan

ARTICLE INFO

Keywords:
Graphite film
Structure
Thermal conductivity
Low energy cost

ABSTRACT

With the rapid development of the electronics industry, the demand for superior heat dissipation materials is increasing. Although many studies have been conducted on graphene films with high thermal conductivity, most of them are processed at high temperatures (~3000 °C) using graphene oxide, which is environmentally harmful and consumes large amounts of energy. This paper reports a simple, low-cost, low-energy, high-efficiency method for the preparation of graphite films using only environmentally friendly materials. Composite films with a thermal conductivity of 298.5 $Wm^{-1}K^{-1}$ were successfully produced by simply dispersing and exfoliating natural graphite and carboxymethylcellulose in a roll mill and depositing by blade coating. Conventional films fabricated using graphene nanoplates (GNP) exhibited a thermal conductivity of 94.6 $Wm^{-1}K^{-1}$, which is significantly lower than the graphite film produced by roll-milling. Experimental and theoretical investigations reveal the reason for this is that the mixed structure of large graphite and small graphite/GNP reduces the interfacial thermal resistance while forming a denser network of heat conduction paths.

1. Introduction

With the rapid development of the electronics industry in recent years, the performance of devices and other components has improved, and the amount of heat generated has risen accordingly. In addition, as devices and electronic components become smaller, heat tends to accumulate more easily. Inadequate heat dissipation leads to reduced device performance and lifetime, so demand for better heat dissipation materials with higher thermal conductivity and lower density is increasing [1–3].

Conventional heat dissipation materials have mainly been metallic materials such as copper and aluminum [4] , but they have the disadvantages of high density and reduced thermal conductivity at decreased thickness. Among the non-metallic materials that have replaced it, graphene is the most investigated [5]. Graphene has a low density (2.2 gcm^{-3}) compared to metals and other materials and, in the case of a single layer graphene, a thermal conductivity reaching 5300 $Wm^{-1}K^{-1}$ at room temperature [6,7] in addition to excellent mechanical properties [8], and is therefore being actively investigated as a next-generation heat dissipation material.

The general consensus is that the thermal conductivity of graphene increases with decreasing number of layers [9,10] and reaches a maximum at a single layer, but this is only true under conditions where the pure graphene is suspended between supports. When graphene is dispersed in a matrix, such as in composites, phonon scattering occurring at the interface actually reduces the thermal conductivity of graphene with decreasing layer number [11] but recovers to values close to those of bulk graphite >30 atomic layers [12]. It has also been reported that the thermal conductivity of graphite flakes increases with particle size [13]. Thus, it appears that thicker and larger graphite is more effective for improving the thermal conductivity of composite films rather than thin graphene.

There are two main methods of existing graphene film production. One is to use graphene oxide (GO) as raw material and produce graphene films by thermal or chemical reduction [14–16]. For example, Peng et al. [14] successfully produced graphene films with a thermal

* Corresponding author at: Waseda University, Department of Applied Mechanics and Aerospace Engineering, 3-4-1, Okubo, Shinjuku, Tokyo, Japan.
E-mail address: arao@waseda.jp (Y. Arao).

https://doi.org/10.1016/j.jcomc.2025.100580

Available online 4 March 2025

conductivity of 1940 $Wm^{-1}K^{-1}$ by thermal reduction of GO (rGO) at 3000 °C. However, the preparation of GO requires the use of strong acids and the resulting wastewater is a major environmental burden. In addition, the extremely high annealing temperature of 3000 °C consumes large amounts of energy and is not cost-effective. There is some research on thermal reduction at relatively low temperatures (~1000 °C), but it is not adequate to fully repair the defects in GO and thus the thermal conductivity is relatively low; these reports confirm that higher annealing temperature is required for recovering higher thermal conductivity [17]. Another is the mechanical exfoliation and dispersion of expanded graphite (EG) or graphene nanoplatelets (GNP) [18–20]. For example, Zhang et al. [18] successfully produced films with 80 % EG loading and a thermal conductivity of 63.9 $Wm^{-1}K^{-1}$ by dispersing EG with cellulose nanofibers (CNF) by sonication and vacuum filtration. This method is less costly than the GO/rGO system, but has a relatively low thermal conductivity and, like GO, EG has an environmental burden due to the use of acid during fabrication. In addition, a disadvantage common to all methods is that the vacuum filtration used in most studies is time-consuming and makes it difficult to produce large-area films.

In this study, only natural graphite and carboxymethylcellulose (CMC) are used as raw materials, without the environmentally harmful GO, EG and strong acids as described above. The process also does not involve annealing at extremely high temperatures, which is both economically and energetically costly, but rather uses a very simple process: exfoliation and dispersion by roll milling, film production by blade coating, and pressing. Three-roll milling is an ideal exfoliation method to produce thin graphite with large lateral size, which is optimal for improving thermal conductivity of films [21,22]. Films prepared with a graphite:CMC mass ratio of 85:15 have a thermal conductivity of 213.2 $Wm^{-1}K^{-1}$ at low density (1.37 gcm^{-3}) without pressing, and films with a maximum density of 1.90 gcm^{-3} and thermal conductivity of 298.5 $Wm^{-1}K^{-1}$ were successfully produced after pressing.

2. Materials and methods

2.1. Materials

Natural graphite (808,113, Aldrich) was chosen as the raw material for this study. Carboxymethylcellulose (F04HC, NIPPON PAPER INDUSTRIES Co., Ltd.) was used as dispersant. Graphene nanoplates (M25, XG-Science) were used for comparison with natural graphite, having an average particle size of 25 μm and thickness of 6–8 nm.

2.2. Production of graphite/CMC composite films (graphite films)

CMC was added to pure water at a mass concentration of 3 % and stirred in a hot stirrer (100 °C, 1400 rpm) for 40 min to produce an aqueous CMC solution. The natural graphite was then mixed into this CMC solution such that the graphite content in the solid fraction was set at 35, 45, 55, 65, 70, 75, 80, 85, and 90 wt% to study the effect of film composition, and stirred in a high speed mixer homogenizer (Spinmix SX10, Mitsui Electric Co., Ltd.) at 5000 rpm for 10 min; a graphite content of 85 wt% was selected to compare the effect of number of passes in the roll mill. The mixture was then dispersed and stripped in a three-roll mill (BR-150HCV III, Aimex Co., Ltd.). A roll mill is a device consisting of three rolls with different rotational speeds (feed roll, center roll and apron roll), as shown in Fig. S1. When the slurry is pushed into the narrow gap between the rolls, the shear forces generated by the speed difference between the rolls overcome the van der Waals forces between the layers of graphite and results in exfoliation with minimal damage, and the degree of exfoliation can be adjusted by controlling the distance between rolls, rotation speed of rolls and number of passes. The mixture was passed through 1, 3, 5, 10, 20 and 30 times (fixed at 10 passes for comparison of graphite content) at a finishing roll speed of 350 rpm and gaps of 20 μm and 10 μm gap on the preparation and finishing sides, respectively. The resulting slurry was degassed with an oil-rotary vacuum pump (AVRD-60A, As One Co., Ltd.) for about 15 min and then the film was fabricated by doctor blade-type sheet forming equipment (DP150, Pacific Tech Co., Ltd.). The blade height was set so that the film thickness after drying is about 100 μm and the film was fed at a speed of 0.8 m/min. The resulting film was dried at room temperature for at least 48 h. Finally, the graphite film was sandwiched between Kapton films with a total thickness of 50 μm and roll-pressed with a gap width of 65 μm. A diagram of these operations is shown in Fig. 1.

2.3. Production of GNP/CMC composite films (GNP films)

CMC was added to pure water at a mass concentration of 3 % and stirred in a hot stirrer (100 °C, 1400 rpm) for 40 min to produce an aqueous CMC solution. The mixture of graphite and CMC solution was prepared so that the graphite content in the solid fraction was 55, 70, and 85 wt% and stirred in a homogenizer at 5000 rpm for 10 min. The resulting slurry was degassed with an oil-rotary vacuum pump (AVRD-60A, As One Co., Ltd.) for about 15 min and then the film is formed by doctor blade type sheet forming equipment (DP150, Pacific Tech Co., Ltd.). The blade height was set so that the film thickness after drying is about 100 μm and the film was fed at a speed of 0.8 m/min. The resulting film was dried at room temperature for at least 48 h. Finally, the GNP film was pressed at 200MPa.

2.4. Characterization

To measure the particle size of the produced graphite, a mixture with an extremely dilute graphite concentration of pure water : CMC : graphite = 20 : 0.1415 : 0.0085 was made after processing with a roll mill, and after film formation and drying by blade coating at a blade height of 0.4 mm, the particle size was measured using a digital 3D microscope (VHX-5000, KEYENCE Co., Ltd) was used to measure the particle size.

To observe the morphology and orientation of graphite, pore morphology and thickness in the prepared films, measurements were made using a Schottky Emission Scanning Electron Microscope (JSM-7001F, JEOL Co., Ltd) and a digital 3D microscope (VHX-5000, KEYENCE Co.,Ltd). The cross sections were produced by 5 h treatment using a cross section polisher (IB-09020CP, JEOL Co., Ltd). To quantitatively measure the orientation of graphite in the produced films, measurements were made using a Automated Multipurpose X-ray Diffractometer With Guidance Software (SmartLab 9 kW, RIGAKU Co.,Ltd)(See S10 for details.).

The viscosity was measured using a viscometer (ASJ-8ST, AS ONE Co., Ltd). The measurement time is 3 min, and the temperature of the sample is controlled within 25 °C ± 1 °C.

Thermal conductivity was measured using a steady-state thermal conductivity measuring device (Fig. S2). The sample shape was a stripe of 2 × 15cm. The amount of heat transferred was calculated from the amount of temperature drop of the heater under steady state conditions, and the thermal conductivity was calculated by dividing the calculated heat transfer amount by the product of the distance and temperature difference between the measuring point and the heater. It is confirmed that the error is within ±5 % by measurements using an aluminum foil.

3. Results and discussion

3.1. Effect of number of passes (Fixed at 85 % graphite content)

Viscosity of a solvent is an important parameter for processability of three-roll milling and doctor blading. The viscosity of a 3 % CMC solution is around 350 Pa·s, and increases to around 500 Pa s after introducing natural graphite with a homogenizer. The viscosity of the slurry after 10 passes in a roll mill further increases to around 2000 Pa·s (Fig. S3). This is presumably due to the increase in specific surface area due to the exfoliation of graphite and the evaporation of water that

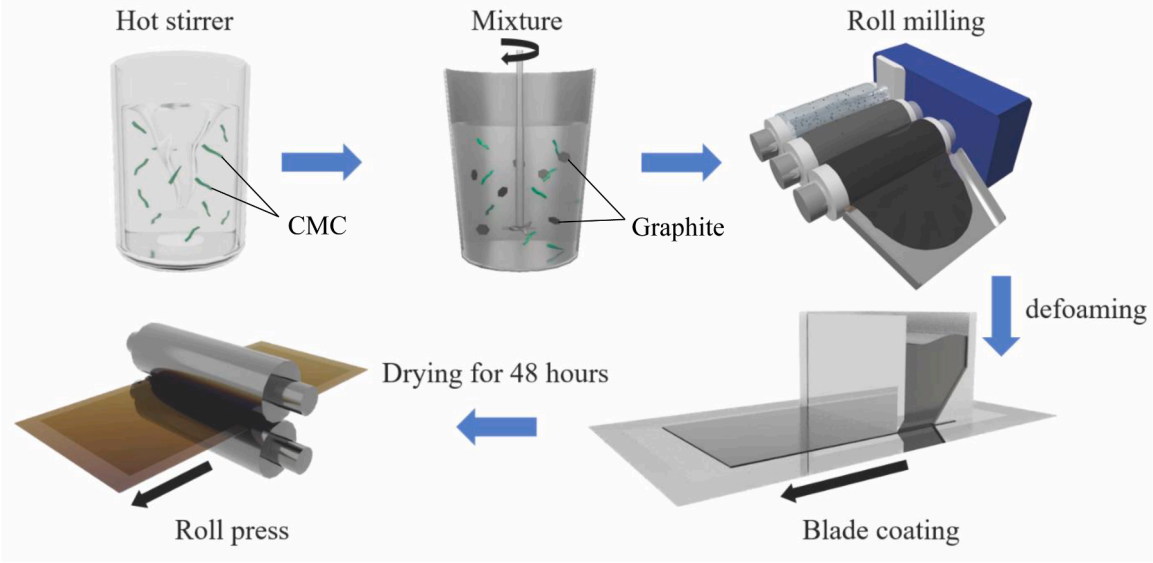

Fig. 1. Schematic diagram of the exfoliation of graphite and film fabrication process.

occurs during roll-milling process. Three-roll milling and blade casting could be conducted without any problems in this range of viscosity change.

Fig. 2(a) shows the film photographed from above in a darkroom with a light source placed under the film, which is a simple method for assessing the dispersion state of graphite in the film. The white areas are voids where neither graphite nor CMC exists, indicating that without the roll milling process, dispersion is extremely poor, resulting in a film full of holes. The large voids almost disappear after three or more passes of roll milling, and large-area robust films with excellent dispersion could be produced by using slurries with three or more passes (Fig. 2(b)). Cross-sectional observation under an optical microscope (Fig. 2(c)) shows that graphite (white regions) appears to agglomerate at a low number of passes, but shows good dispersion as a mixture of thin and thick sheets as the number of passes increases, with a consistent orientation in the in-plane direction. The thickness of each film was measured at 30 locations and their average, maximum and minimum values are shown in Fig. 2(d). As per the cross-sectional observation, there is a large variation in film thickness up to 5 passes, but after 10 passes, the variation in thickness is much smaller.

The particle size distribution measured by optical microscopy showed that 98.6 % of the particles were <15 μm (Fig. S4(d)). Direct observation of the sheets remaining on the grid using TEM revealed an average particle size of 8.55 μm and a thickness of 8.90 nm (Fig. S5(a-d)). In terms of the number of particles, it is clear that the graphite was converted to GNP by roll milling. On the other hand, from the cross-sectional observation in Fig. 2(c), it is also clear that large graphite particles occupy a significant portion of the material volume. Therefore, when taking the aspect ratio of the graphite to be 1000 and converting cumulative particle distribution and size to volume content, it was found that a large volume was occupied by graphite with a large particle size, as shown in Fig. 3(a). In fact, when the large graphite was removed by centrifugation (1000 rpm, 10 min) after roll milling, the concentration of GNP in the supernatant solution was 2.05 %, indicating a significant proportion of total graphite volume consists of large particles (Fig. S5 (e)). This is also consistent with the cross-sectional observation in Fig. 2 (c). It is evident that the roll milling results in a mixed structure of graphite and GNP. The damage caused by the roll milling was estimated by Raman to be 0.026 in terms of I_D/I_G, confirming that there is little damage to the graphite surface (Fig. S6).

It is known that the thermal conductivity of graphite/graphene films is strongly influenced by the density. Therefore, the density was measured before and after pressing, as shown in Fig. 3(b). Even without pressing, it is clear that the density increased with increasing number of roll mill passes. This is because the thinned sheets are able to fill the gaps between the larger graphite particles and improve packing efficiency, which increases the density with increasing number of passes. Conversely, only a slight increase in density was observed for increasing number of passes when the films were pressed, reaching a higher density of 1.7 gcm^{-3} after 3 passes and approaching the theoretical value. The thermal conductivities of the films are shown in Fig. 3(c). The increase in thermal conductivity tended to saturate after 10 passes, which is because the increase in density and dispersibility was counteracted by the decrease in particle size. Considering the labor and energy consumption of roll milling, the optimum number of passes is 10, and all the proceeding investigations of graphite content effect employed 10 passes.

3.2. *Effect of graphite content*

From this, samples with graphite as raw material are referred to as 'Gr+number' and samples with GNP as raw material as 'GNP+number', where the numbers indicate the graphite content. In comparison with graphite content, the thermal conductivity generally increased with increasing graphite content, regardless of pressing, and a maximum thermal conductivity of 298.5 $Wm^{-1}K^{-1}$ and density of 1.90 gcm^{-3} was obtained at 85 % graphite content (Fig. 4(a and b)). Gr90 have a low density of 1.69 gcm^{-3} because of its low strength will cause it to fracture under excessive pressing; however, if it could somehow be pressed to the same level as Gr85, a higher thermal conductivity can be expected. The density of the films containing GNP was low before pressing (at 0.3–0.5 gcm^{-3}) and decreased with increasing GNP content. The density of roll-milled exfoliated films was 1–1.5 gcm^{-3}, which is higher than that of GNP. It is assumed that this is mainly due to the viscosity of the slurry, with GNP having a higher viscosity due to its higher specific surface area and a smaller reduction in thickness on moisture volatilization. After pressing, the density of GNP films was 1.7 gcm^{-3}, which was the same or slightly lower than that of film produced by roll mill exfoliation. In terms of thermal conductivity, the GNP film reached a maximum value of about 90 $Wm^{-1}K^{-1}$ at 85wt%, while Zhang et al. [10] measured the thermal conductivity of a film made of GNP and cellulose nanofibers and obtained a value of 69.3 $Wm^{-1}K^{-1}$, which is in general agreement with our GNP/CMC composite film. For films prepared by roll-mill exfoliation, the thermal conductivity is 295 $Wm^{-1}K^{-1}$ at 85wt%, which is three times higher than that obtained with GNP, meaning that higher thermal

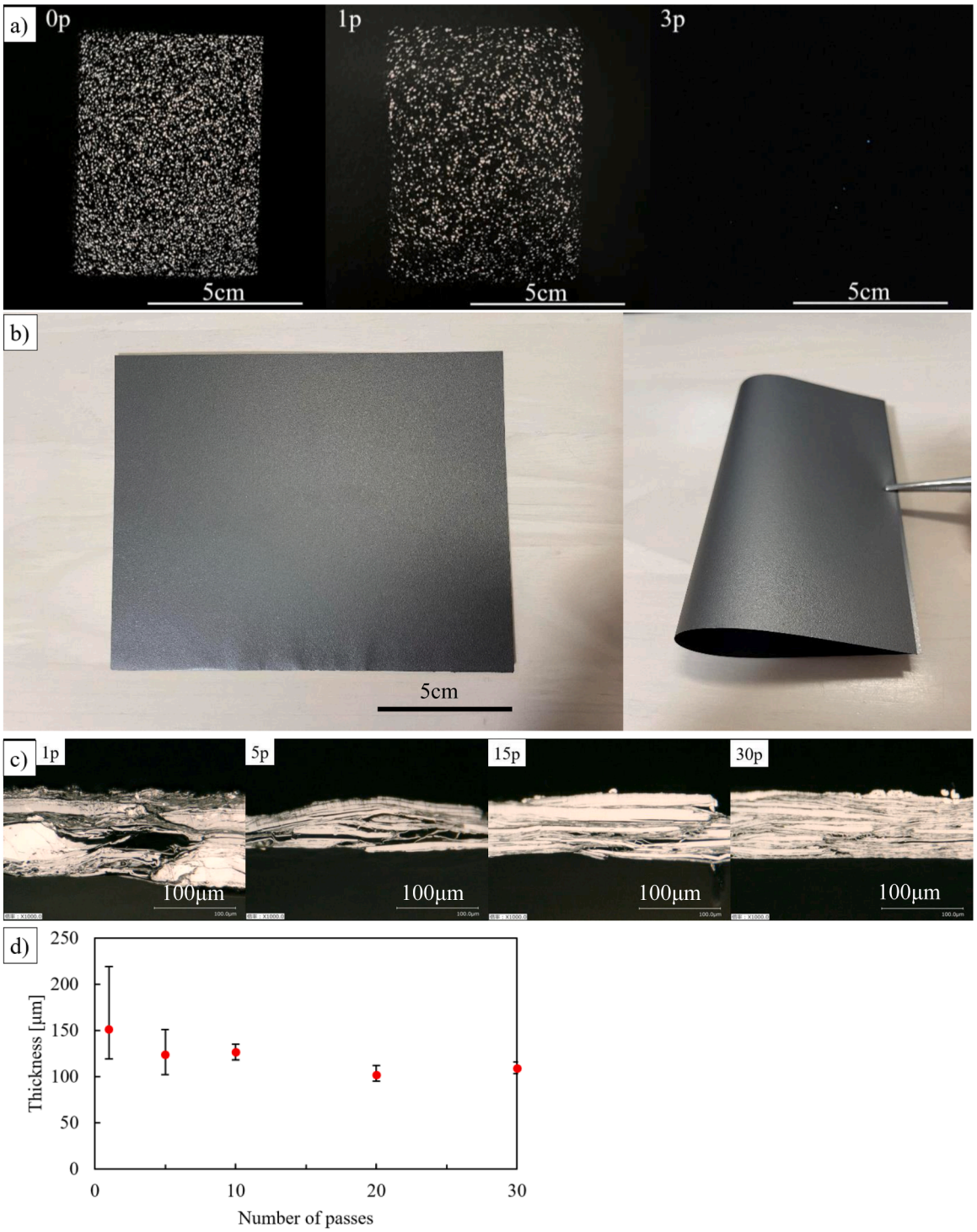

Fig. 2. Structure of exfoliated graphite films with different number of passes of roll milling. a) Void distribution of the films, b) Visual image of large-area exfoliated graphite film(10pass), c) Optical microscope images of cross-sections (before press), d) Film thickness with different pass count.

conductivity is obtained with a mixed structure of graphite and GNP sheets rather than with GNP alone. Fig. 4(c and d) shows the cross sections of pressed films containing 85 % graphite or GNP as observed by optical microscopy, which are schematically illustrated in Fig. 4(e and f). The film produced from roll milling natural graphite consists of small, thin graphite flakes/GNP packed between larger, thicker graphite flakes, resulting in well-formed network paths for heat conduction and thus exhibits the highest thermal conductivity in this study. The high degree of orientation and size of graphite flakes significantly reduce the influence of phonon scattering and interfacial thermal resistance—even after 30 passes, over 98 % of particles have >180 layers (see Fig. S7(e)). By comparison, the film containing GNP (Fig. 4(f)) had a relatively low thermal conductivity due to the slightly lower degree of orientation and the greater influence of interfacial thermal resistance and phonon scattering in the thin sheets. The likely reason for the lower orientation is the large number of voids and low density before pressing, which prevented high orientation even after pressing. This is further apparent when comparing the films using thermography as shown in Fig. 5(a).

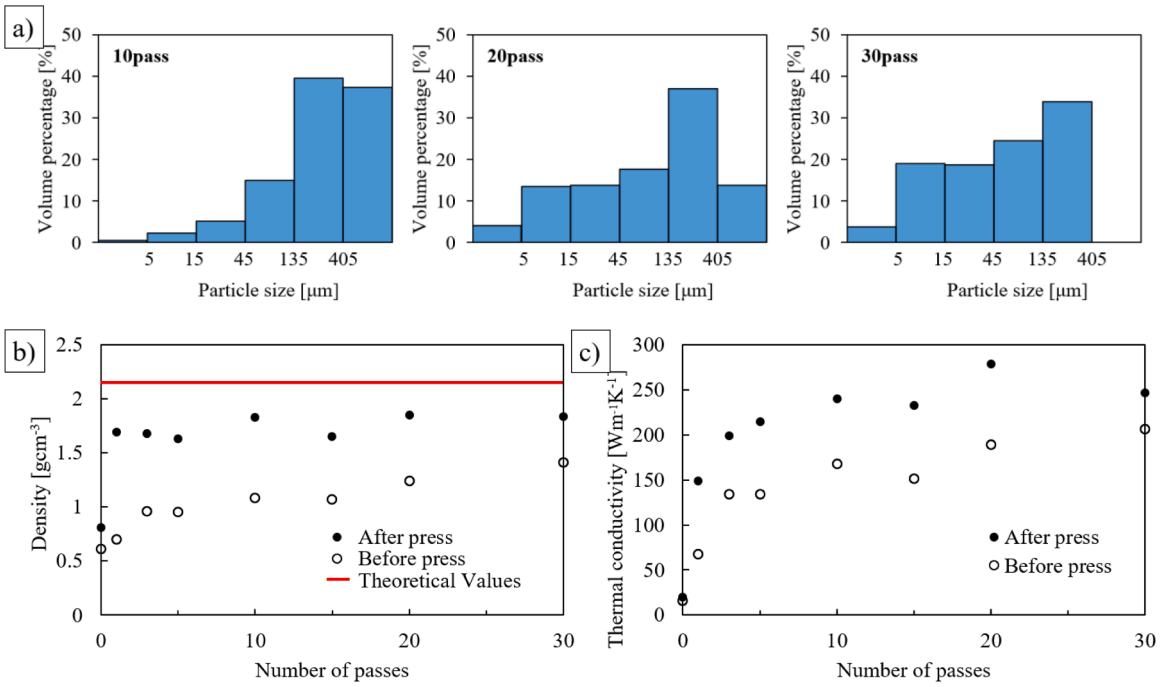

Fig. 3. Particle size and density and thermal conductivity of exfoliated graphite films with different number of passes. (1 pass is defined as the number of times when the mixture is fed into the roll mill between feed roll and center roll until it is all collected from the blade of the apron roll.

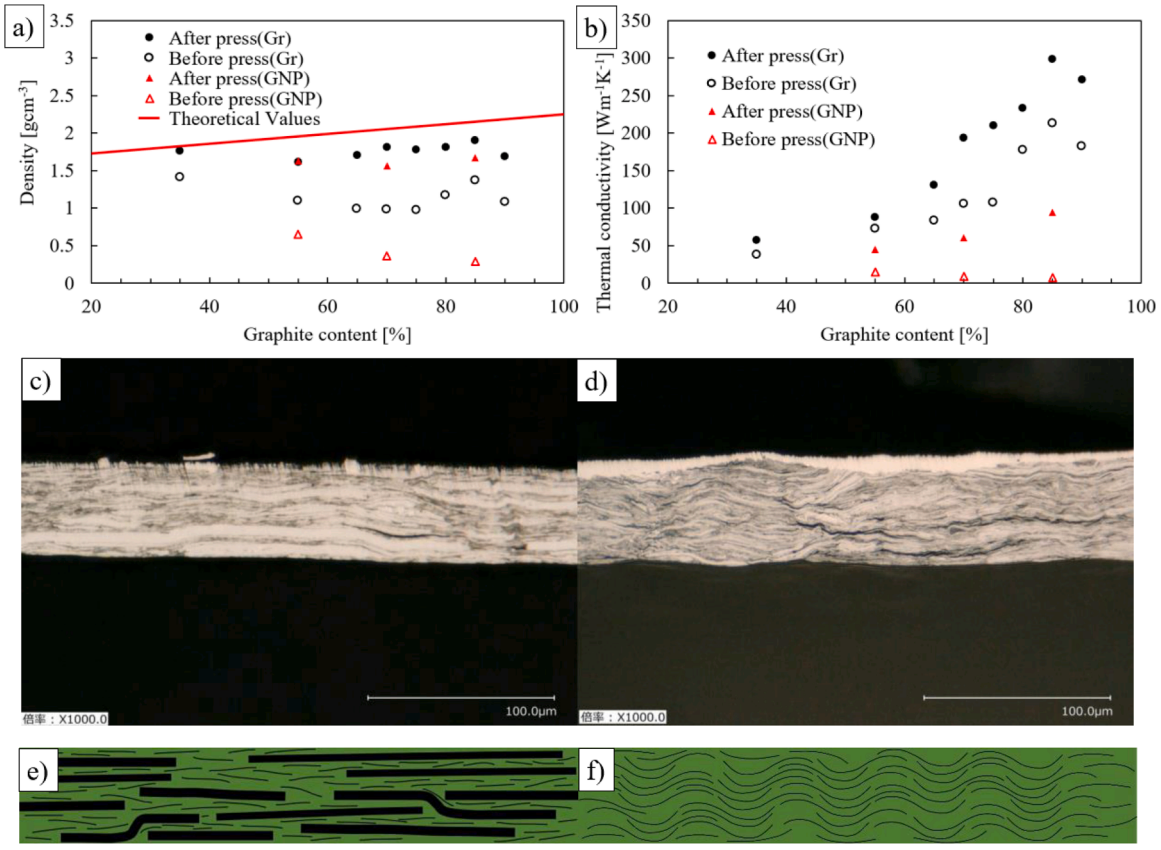

Fig. 4. Comparison of the structure and properties of exfoliated graphite and GNP with different filler content. a) Density, b) Thermal conductivity, c) Optical microscope images of cross-sections (graphite content 85 %, after press), d) Optical microscope images of cross-sections (GNP content 85 %, after press), e) Schematic of cross section (thin graphite flakes between thick graphite flakes), f) Schematic of cross section (only GNP).

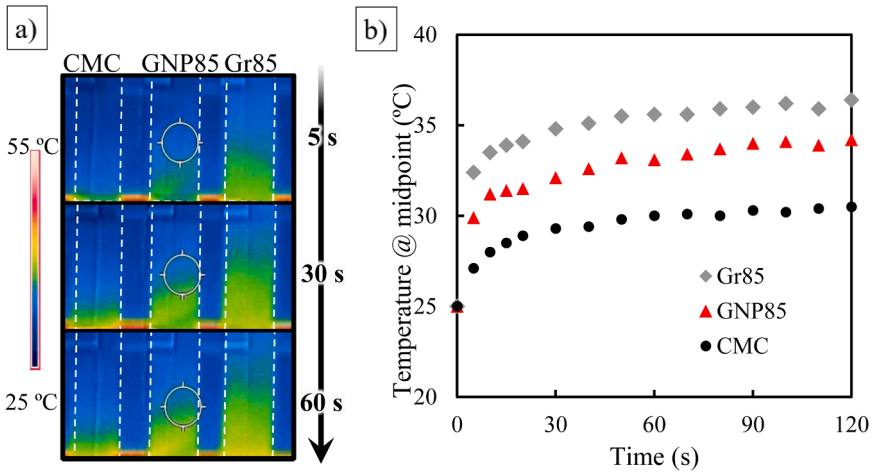

Fig. 5. Comparison of exfoliated graphite and GNP use thermography. a) Results of thermography, b) Temperature variation at sample midpoint.

Compared to CMC and GNP85 films, yellow area of Gr85films (roll milled graphite) increased with time, indicating that temperate from the heat source is transferred well. Fig. 5(b) shows the temperature change over time at the midpoint between the heat source and sink. Temperature at the midpoint of the graphite film is 2.5 °C higher than the GNP film after only 5 s. These results are consistent with in-plane thermal conductivity measurements (Gr85: 295Wm^{-1}K^{-1}, GNP: 90Wm^{-1}K^{-1}).

3.3. Model-based calculations

The Lin et al. model [23] is used to calculate the in-plane thermal conductivity of the films in this study, which takes into account of shape, orientation, thermal conductivity anisotropy and interfacial thermal resistance of the filler in the composite material. The theoretical equations are as in Eqs. (1)-(6):

$$K_{e11} = K_{e22} = K_m \frac{2 + f[\beta_{11}(1 - L_{11})(1 + \langle\cos^2\theta\rangle) + \beta_{33}(1 - L_{33})(1 - \langle\cos^2\theta\rangle)]}{2 - f[\beta_{11}L_{11}(1 + \langle\cos^2\theta\rangle) + \beta_{33}L_{33}(1 - \langle\cos^2\theta\rangle)]} \tag{1}$$

$$K_{e33} = K_m \frac{1 + f[\beta_{11}(1 - L_{11})(1 - \langle\cos^2\theta\rangle) + \beta_{33}(1 - L_{33})\langle\cos^2\theta\rangle]}{1 - f[\beta_{11}L_{11}(1 - \langle\cos^2\theta\rangle) + \beta_{33}L_{33}\langle\cos^2\theta\rangle]} \tag{2}$$

$$\beta_{ii} = \frac{K'_{fii} - K_m}{K_m + L_{ii}\left(K'_{fii} - K_m\right)} \tag{3}$$

$$L_{11} = L_{22} = \frac{p^2}{2(p^2 - 1)} + \frac{p}{2(1 - p^2)^{3/2}}\cos^{-1}p \tag{4}$$

$$L_{33} = 1 - 2L_{11} \tag{5}$$

$$K'_{f11} = K'_{f22} = \frac{B}{2R_k + B/K_{f11}} \tag{6}$$

where $K_{e11}(=K_{e22})$ is the thermal conductivity of the composite in the in-plane direction, K_{e33} is the thermal conductivity of the composite in the out-of-plane direction, f is the volume fraction of the filler, K_m is the thermal conductivity of the matrix, $K_{f11}(=K_{f22})$ is the theoretical thermal conductivity of the filler in the in-plane direction, K_{f33} is the theoretical thermal conductivity of the filler in the out-of-plane direction, p is the inverse of the filler aspect ratio (thickness/particle size), $\langle\cos^2\theta\rangle$ is the statistical orientation of the filler, R_k is the interfacial thermal resistance.

However, the particle size distribution of graphite particles in the films produced in this study is very wide and the discrepancy between experimental and theoretical values is very large when calculated using a single particle size, so calculations are performed using multiple particle sizes. The thermal conductivity of composites containing particles of several different sizes can be calculated by assuming that the thermal conductivity of each particle size is calculated using the model of Lin et al. in series with its volume fraction, as expressed by Eq. (7):

$$K_C = \frac{100\%}{\sum_{i=1}^{n} f_i K_i} \tag{7}$$

where K_C is the thermal conductivity of the composite in the in-plane direction, K_i is the Thermal conductivity in the in-plane direction calculated for each particle size, f_i is the volume fraction of each type of particle.

Material constants and conditions are listed in Table S1. As the interfacial thermal resistance could not be measured, it was set as a fitting parameter so that the calculated values fit the experimental values. Catalogue values are used for GNP particle size and aspect ratio, while the particle size of the exfoliated graphite is based on the actual measurements from the 10 passes case (Fig. 3(a)), calculated as the average particle size and volume fraction of the six particle size ranges; the specific values are listed in Table S2. All other conditions are close to the measured values and the calculated results are shown in Fig. 6. The interfacial thermal resistance of the graphite film (5.0×10^{-8} m^{2}KW^{-1}) was 33 % lower than the GNP film (7.5×10^{-8} m^{2}KW^{-1}), as it contains more highly oriented particles that are also less likely to fold and wrinkle (Fig. S11), in addition to having fewer micro voids in the film structure. These values are larger than those reported in the literature for

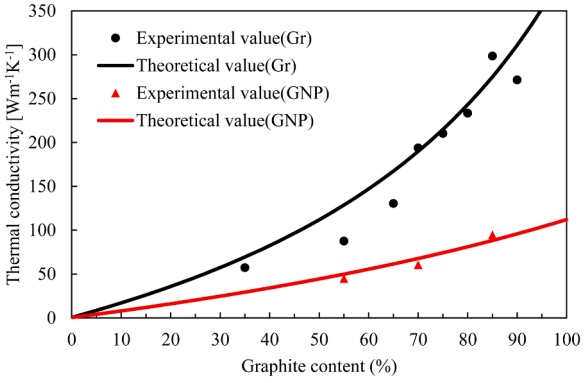

Fig. 6. Comparison of theoretical and experimental values of thermal conductivity.

graphene/polymer systems with perfect-interface assumption (0.6–1.7 $\times 10^{-8}$ m^2KW^{-1}) [24–30]; this is likely due to the micro voids and particle folding/wrinkling found in the present study, as mentioned above, which are known to contribute to the apparent interfacial thermal resistance. In order to investigate which parameter has the greatest influence on thermal conductivity, Fig. S8 shows calculated values of thermal conductivity of the GNP film when each parameter was replaced by that the graphite film, indicating that the particle size has the greatest influence on thermal conductivity. Larger particles with a larger volume fraction can significantly reduce the number of interfaces, resulting in a significant reduction in the effect of interfacial thermal resistance and a significant increase in thermal conductivity, even if the values for interfacial thermal resistance are the same. In order to investigate the effect of different particle size distributions on thermal conductivity for the same average particle size in a unit volume ($\sum_{i=1}^{n} f_i B_i = 271[\mu m]$), the results of calculations varying only the particle size used in the theoretical calculations for graphite are shown in Fig. S9. The particle size distribution used in the calculations is shown in Table S3, which shows that the broader the particle size distribution, the lower the thermal conductivity. The sharper size distribution results in higher thermal conductivity. Uniform size distribution is beneficial to reduce the surface are of graphite flakes in ideal materials; hence reducing the phonon scattering at the interface. However, in real materials, dispersion of only large particle size of graphite results in the formation of voids in the films, which lead to reduction of thermal conductivity (Figs. 2(a) and Fig. 3(c)). Therefore, a mixture of large graphite and small graphite/GNP is beneficial in improving thermal conductivity of the actual films.

3.4. Comparison with other studies

A comparison of the results of this study with those of other studies is shown in Fig. 7 [31–43]. It should be noted that most of reference data were obtained by thermal diffusivity measurement using laser flash method. We have compared the two methods, the steady-state method and the Angstrom method, which is a non-steady-state method like laser flash method, and found that there was no significant difference between them, with the steady-state method obtaining data with less variation. All studies reporting values above 500 $Wm^{-1}K^{-1}$ have used free-standing rGO, but as mentioned above, these methods have significant disadvantages such as high environmental burden and cost, and the films do not contain binders. Comparing this study with GNP-based films (black markers), this study showed considerably higher values for all particle loadings, especially in the high content region. The underlying reason for this is that similar studies all used GNP/few-layer graphene, whereas this study utilized graphite of which >98 % (by volume) had a thickness of 60 nm or more, and >80 % had a particle size of 135 μm or more. As mentioned above, when graphene is supported by, such as in composites, due to phonon interfacial scattering, graphene with fewer layers shows lower thermal conductivity than graphite, and larger graphite can also reduce the effect of interfacial thermal resistance, so this study is superior to other studies using graphene, which has fewer layers and is relatively small. However, films that include only large graphite particles will contain many voids due to limited packing efficiency, making it difficult to form thermal conduction paths, so thin and small graphite/GNP particles are also needed to fill the gaps between large particles and create a dense structure with more thermal conduction paths. The mixed structure of large graphite and small graphite/GNP has enabled thermal conductivity comparable to that of metals such as aluminum to be obtained without the need for high temperature annealing.

4. Conclusion

This study succeeded in producing films with the highest thermal conductivity of any similar study, using only roll-milling and blade-coating methods, which are environmentally friendly and suitable for industrial production. The roll-milling process significantly reduced the voids in the film and increased dispersion and orientation, leading to a significant increase in thermal conductivity and reaching a maximum value of 298.5 $Wm^{-1}K^{-1}$ for pressed films with 85 % graphite content. Furthermore, even films with low density and low graphite content exhibited higher thermal conductivities compared to similar materials in the literature. We have verified that a structure combines large graphite and small graphite/graphene nanoplatelets improves in-plain thermal conductivity of the films, due to low interfacial thermal resistance of thick graphite and good thermal conductive pass produced by thin graphene nanoplatelets.

CRediT authorship contribution statement

Junhao Wang: Writing – original draft, Investigation, Formal analysis, Data curation. **Hongsheng Lin:** Investigation, Data curation. **Jonathon D. Tanks:** Writing – review & editing, Supervision, Data curation. **Yoshihiko Arao:** Writing – review & editing, Supervision, Resources, Project administration, Investigation, Funding acquisition,

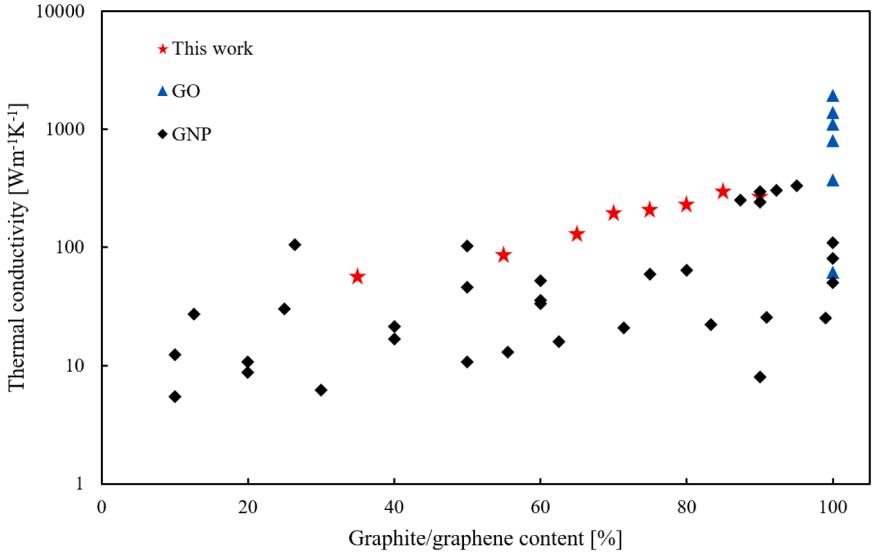

Fig. 7. Comparison of this work with other works. [14–16,18–20,31–44].

Conceptualization.

Declaration of competing interest

The authors declare the following financial interests/personal relationships which may be considered as potential competing interests:

Yoshihiko Arao reports financial support was provided by Japan Society for the Promotion of Science. If there are other authors, they declare that they have no known competing financial interests or personal relationships that could have appeared to influence the work reported in this paper.

Acknowledgments

This work was the result of using research equipment (G1016, G1023, G1039) shared in MEXT Project for promoting public utilization of advanced research infrastructure (Program for supporting construction of core facilities) Grant Number JPMXS0440500024.

This work was supported by JSPS KAKENHI Grant Number 22H00189.

Supplementary materials

Supplementary material associated with this article can be found, in the online version, at doi:10.1016/j.jcomc.2025.100580.

Data availability

Data will be made available on request.

References

[1] AA. Balandin, Thermal properties of graphene and nanostructured carbon materials, Nat. Mater. 10 (8) (2011) 569–581.
[2] W. Feng, M. Qin, Y. Feng, Toward highly thermally conductive all-carbon composites: structure control, Carbon N Y 109 (2016) 575–597.
[3] AL. Moore, Li Shi, Emerging challenges and materials for thermal management of electronics, Mater. Today 17 (4) (2014) 163–174.
[4] X. Qu, et al., Review of metal matrix composites with high thermal conductivity for thermal management applications, Prog. Nat. Sci.: Mater. Int. 21 (3) (2011) 189–197.
[5] A.K. Geim, Graphene: status and prospects, Science 324 (5934) (2009) 1530–1534.
[6] AA. Balandin, et al., Superior thermal conductivity of single-layer graphene, Nano. Lett. 8 (3) (2008) 902–907.
[7] D.S. Ghosh, et al., Extremely high thermal conductivity of graphene: prospects for thermal management applications in nanoelectronic circuits, Appl. Phys. Lett. 92 (15) (2008) 151911.
[8] C. Lee, et al., Measurement of the elastic properties and intrinsic strength of monolayer graphene, Science 321 (5887) (2008) 385–388.
[9] S. Ghosh, et al., Dimensional crossover of thermal transport in few-layer graphene, Nat. Mater. 9 (7) (2010) 555–558.
[10] DL. Nika, AA. Balandin, Two-dimensional phonon transport in graphene, J. Phys. Condens. Matter 24 (23) (2012) 233203.
[11] W. Jang, et al., Thickness-dependent thermal conductivity of encased graphene and ultrathin graphite, Nano Lett. 10 (10) (2010) 3909–3913.
[12] M.M. Sadeghi, I. Jo, Li Shi, Phonon-interface scattering in multilayer graphene on an amorphous support, Proc. Natl Acad. Sci. 110 (41) (2013) 16321–16326.
[13] DL. Nika, AS. Askerov, AA. Balandin, Anomalous size dependence of the thermal conductivity of graphene ribbons, Nano Lett. 12 (6) (2012) 3238–3244.
[14] Li Peng, et al., Ultrahigh thermal conductive yet superflexible graphene films, Adv. Mater. 29 (27) (2017) 1700589.
[15] G. Xin, et al., Large-area freestanding graphene paper for superior thermal management, Adv. Mater. 26 (26) (2014) 4521–4526.
[16] P. Kumar, et al., Large-area reduced graphene oxide thin film with excellent thermal conductivity and electromagnetic interference shielding effectiveness, Carbon N Y 94 (2015) 494–500.
[17] N.-J. Song, et al., Thermally reduced graphene oxide films as flexible lateral heat spreaders, J. Mater. Chem. A 2 (39) (2014) 16563–16568.
[18] Bo Zhang, Z. Li, L. Wang, Effect of lateral size and loading ratio of expanded graphite on mechanical and thermal properties of nanocellulose composites, Mater. Today Comm. 33 (2022) 104549.
[19] M. Zhang, et al., Enhanced thermal conductivity and lower density composites with brick-wall microstructure based on highly oriented graphite nanoplatelet: towards manufacturable cooling substrates for high power density electronic devices, Nanotechnology 30 (24) (2019) 245204.
[20] G. Li, et al., Fabrication of robust and highly thermally conductive nanofibrillated cellulose/graphite nanoplatelets composite papers, Compos. Sci. Technol. 138 (2017) 179–185.
[21] M. Liu, et al., A novel approach to prepare graphite nanoplatelets exfoliated by three-roll milling in phenolic resin for low-carbon MgO-C refractories, J. Eur. Ceram. Soc. 43 (2023) 4198–4208.
[22] X. Yang, et al., Design and preparation of multiple, multidimensional and multiscale Ni/GC/CNTs/MLGs toughened phases, Ceram. Int. 50 (2024) 36320–36329.
[23] W. Lin, R. Zhang, C.P. Wong, Modeling of thermal conductivity of graphite nanosheet composites, J. Electron. Mater. 39 (3) (2010) 268–272.
[24] T. Luo, JR. Lloyd, Enhancement of thermal energy transport across graphene/graphite and polymer interfaces: a molecular dynamics study, Adv. Funct. Mater. 22 (12) (2012) 2495–2502.
[25] L. Hu, T. Desai, P. Keblinski, Determination of interfacial thermal resistance at the nanoscale, Phys. Rev. B—Condensed Matter Mater. Phys. 83 (19) (2011) 195423.
[26] A. Verma, R. Kumar, A. Parashar, Enhanced thermal transport across a bi-crystalline graphene–polymer interface: an atomistic approach, Phys. Chem. Chem. Phys. 21 (11) (2019) 6229–6237.
[27] Yu Wang, et al., A molecular dynamics study on thermal and mechanical properties of graphene–paraffin nanocomposites, RSC advance 5 (101) (2015) 82638–82644.
[28] J. Wang, et al., The effects of temperature and alignment state of nanofillers on the thermal conductivity of both metal and nonmetal based graphene nanocomposites, Acta Mater. 185 (2020) 461–473.
[29] L. Zhang, L. Liu, Hierarchically hydrogen-bonded graphene/polymer interfaces with drastically enhanced interfacial thermal conductance, Nanoscale 11 (8) (2019) 3656–3664.
[30] Y. Xiong, et al., Toward improved thermal conductance of graphene-polyethylene composites via surface defect engineering: a molecular dynamics study, Acta. Phys. Chim. Sin 35 (10) (2019) 1150–1156.
[31] B. Shen, W. Zhai, W. Zheng, Ultrathin flexible graphene film: an excellent thermal conducting material with efficient EMI shielding, Adv. Funct. Mater. 24 (28) (2014) 4542–4548.
[32] S. Lin, et al., Ultrathin flexible graphene films with high thermal conductivity and excellent EMI shielding performance using large-sized graphene oxide flakes, RSC Adv. 9 (3) (2019) 1419–1427.
[33] S. Jin, et al., Effects of reduction methods on the structure and thermal conductivity of free-standing reduced graphene oxide films, Diam. Relat. Mater. 58 (2015) 54–61.
[34] JD. Renteria, et al., Strongly anisotropic thermal conductivity of free-standing reduced graphene oxide films annealed at high temperature, Adv. Funct. Mater. 25 (29) (2015) 4664–4672.
[35] Y. Zhang, et al., Characterization and simulation of liquid phase exfoliated graphene-based films for heat spreading applications, Carbon N Y 106 (2016) 195–201.
[36] Z. Wang, et al., One-step scalable preparation of graphene nanosheets and high-thermal-conductivity flexible graphene films, Ceram. Int. 46 (17) (2020) 26760–26766.
[37] Na Song, et al., Anisotropic thermally conductive flexible films based on nanofibrillated cellulose and aligned graphene nanosheets, J. Mater. Chem. C 4 (2) (2016) 305–314.
[38] D. Jiao, et al., Enhanced thermal conductivity in oriented cellulose nanofibril/graphene composites via interfacial engineering, Compos. Comm. 31 (2022) 101101.
[39] Bo Zhang, et al., High-performance cellulose nanofiber-derived composite films for efficient thermal management of flexible electronic devices, Chem. Eng. J. 439 (2022) 135675.
[40] H. Jiang, et al., Light-weight, flexible, low-voltage electro-thermal film using graphite nanoplatelets for wearable/smart electronics and deicing devices, J. Alloys Compd. 699 (2017) 1049–1056.
[41] W. Yang, et al., Completely green approach for the preparation of strong and highly conductive graphene composite film by using nanocellulose as dispersing agent and mechanical compression, ACS Sustain. Chem. Eng. 5 (10) (2017) 9102–9113.
[42] W. Yang, et al., Strong and highly conductive graphene composite film based on the nanocellulose-assisted dispersion of expanded graphite and incorporation of poly (ethylene oxide), ACS Sustain. Chem. Eng. 7 (5) (2019) 5045–5056.
[43] Z. Dai, et al., High-directional thermally conductive stearic acid/expanded graphite-graphene films for efficient photothermal energy storage, Chem. Eng. J. 484 (2024) 149203.
[44] J. Ning, et al., Constructing micro-region networks in expanded graphite for bi-directional high thermal conductivity of thermoplastic polymer composite, Chem. Eng. J. 502 (2024) 158110.